Materials Today Communications 38 (2024) 108402

Contents lists available at ScienceDirect

Materials Today Communications

journal homepage: www.elsevier.com/locate/mtcomm

Development and characterizations of low-modulus Ti–Nb–Cu alloys with enhanced antibacterial activities

Qiang Li [a,b,*], Qizhen Peng [a], Qi Huang [a], Mitsuo Niinomi [a,c,d], Takuya Ishimoto [e], Takayoshi Nakano [d]

[a] School of Mechanical Engineering, University of Shanghai for Science and Technology, Shanghai 200093, PR China
[b] Shanghai Engineering Research Center of High-Performance Medical Device Materials, Shanghai 200093, PR China
[c] Institute for Materials Research, Tohoku University, 2–1–1, Katahira, Aoba-ku, Sendai 980–8577, Japan
[d] Division of Materials and Manufacturing Science, Graduate School of Engineering, Osaka University, 2–1, Yamada-Oka, Suita, Osaka 565–0871, Japan
[e] Institute of Light Metals, Faculty of Sustainable Design, University of Toyama, Toyama, 930–8555, Japan

ARTICLE INFO

Keywords:
Biomedical Ti alloys
Mechanical properties
Corrosion resistance
Cytotoxicity
Antibacterial properties

ABSTRACT:

Avoiding infection is a requirement for the long-term stability and safety of implants, but most Ti alloys for implantation hardly inhibit the bacterial proliferations. Cu works as a β stabilizer in Ti alloys, and Cu ion can kill bacteria. To obtain antibacterial activities in low-modulus Ti alloys, Ti–35Nb–(0, 1, 2, 3, 4)Cu (wt%) alloys were prepared by non-consumable arc melting following by homogenization, hot rolling, and solution treatment. They were then subjected to phase analysis, microstructure observation, tensile test and dynamic polarization. The cytotoxicity and antibacterial activities were finally evaluated. The results show that Cu stabilizes the β phase and inhibits the generation of α" phase during quenching. Ti–35 Nb and Ti–35Nb–1Cu consist of β and α" phases, and Ti–35Nb–(2, 3, 4)Cu alloys have a single β phase. The Ti–Nb–Cu alloys exhibit the Young's moduli ranging from 57 to 72 GPa. All the alloys show passivation behavior with a low passive current density. Cytotoxicity is hardly observed in the alloys. The antibacterial rates of Ti–35Nb–(1, 2, 3, 4)Cu alloys against *E. coli* are 62.8%, 68.9%, 70.9% and 73.2%, respectively, and the antibacterial rates against *S. aureus* are 63.4%, 69.7%, 72.8% and 74.7%, respectively. The developed β-type Ti–35Nb–4Cu alloy shows a relatively low Young's modulus and good antibacterial properties, and is a candidate for biomedical applications.

1. Introduction

Biomaterials have attracted widespread attentions with the developments of materials science and technology. Ti and Ti alloys are commonly employed as orthopedic implants because of their low density, high specific strength, exceptional corrosion resistance and low Young's modulus. However, numerous studies have indicated that the mechanical properties of commercially pure Ti (CP Ti) could not meet the requirements of load-bearing implants [1–3]. Then, Ti–6Al–4 V with good comprehensive mechanical properties has been used as a substitute material for hard tissues [4]. Unfortunately, the Young's moduli of both CP Ti and Ti–6Al–4 V are much higher than that of human bone, which may cause stress shielding [5,6]. Moreover, concerns have been raised regarding the possible long-term implantation complications of Ti–6Al–4 V due to the release of Al and V ions [7,8]. Consequently, recent researches about biomedical Ti alloys significantly focus on β-type Ti alloys, that contain non-toxic elements like Nb, Zr, Ta, Sn, and Mo, and possess low Young's moduli and exceptional biocompatibility. Ti–Nb-based alloys are the most widely developed β-type Ti alloys with low moduli for biomedical applications, such as Ti–29Nb–13Ta–4.6Zr [9], Ti–35Nb–7Zr–5Ta [10], and Ti–24Nb–4Zr–8Sn [11].

Bacterial infections are a serious complication after operation, which may even lead to implant failure [12,13]. Preventing bacterial-associated infections remains a challenge in high-quality health care. In addition to the use of antibiotics during surgery, another method to reduce bacterial infections is using the implants with antibacterial activities. Ag, Cu, and Zn have been used as antibacterial elements [14,15]. However, Ag is expensive and may cause some biosafe problems [16]. The boiling point of Zn is much lower than the melting point of Ti, resulting in an uncontrollable loss during melting. Cu is a low-cost element, and can effectively improve the antibacterial properties of alloys. The formation of bacterial biofilm was inhibited in the

* Corresponding author at: School of Mechanical Engineering, University of Shanghai for Science and Technology, Shanghai 200093, PR China.
E-mail addresses: jxli@tju.edu.cn, liqiang@usst.edu.cn (Q. Li).

https://doi.org/10.1016/j.mtcomm.2024.108402
Received 12 December 2023; Received in revised form 24 January 2024; Accepted 16 February 2024
Available online 17 February 2024

Cu added 317 L stainless steel and Co–Cr-based alloys, promising their applications in the clinical field [17,18]. For Ti alloys, Cu works as a β stabilizer, which can reduce the β transus temperature and increase the β phase stability [19]. Enhanced antibacterial properties were obtained in some Ti alloys by adding Cu, such as Ti–6Al–4V–5Cu and Ti–15Zr–(3, 5, 7)Cu [20,21]. Unfortunately, excessive Cu addition in Ti alloys reduces the plasticity, and desirable mechanical properties including a low modulus, high strength, and suitable plasticity are still research objectives of Cu added antibacterial Ti alloys [22].

Ti–35 Nb (wt%, Ti–22 Nb in at%) with α"+β phases shows a stress-induced martensite transformation during tension [23,24]. Large super-elasticity and low Young's modulus are obtained by adding elements to Ti–35 Nb, such as Ta, Zr, and Cr [25–27]. In this study, Cu was added to Ti–35 Nb to enhance the β phase stability and get some antibacterial activities, and the phase, microstructures, mechanical properties and cytotoxicity were also characterized and analyzed.

2. Materials and methods

2.1. Alloy preparations

Ti–35Nb–(0, 1, 2, 3, 4)Cu (wt%) alloys were fabricated via non-consumable arc-melting under an Ar atmosphere by blending high-purity Ti (≥ 99.99%), Nb (≥ 99.95%), and Cu (≥ 99.95%). The ingots were homogenized at 1000 °C for 12 hours following by water quenching, and then hot rolled at 1000 °C to 2.2 mm-thick sheets under a total reduction of ~83%. The testing samples were cut by wire electrical discharge machining, and subsequently subjected to solution treatment at 800 °C for 1 hour. The oxide layers were ground off after each heat treatment.

2.2. Phase and microstructure characterizations

The samples were scanned by using a Bruker D8 Advance X-ray diffractometer (XRD) with Cu-Kα1 radiation at a speed of 0.1 °/s over a range of 30–80 °, and the current and voltage were 40 mA and 40 kV, respectively. For optical microstructure observation, the samples were inserted in resin, gradually grounded with sandpaper, polished to the mirror surface by SiO_2 solution, and finally etched in a corrosion solution with 94 mL of distilled water, 2 mL of HF, and 4 mL of HNO_3.

2.3. Tensile tests

The dog-bone-shaped samples with the gauge section of 12 mm × 3 mm × 1.5 mm were subjected to tensile tests under room temperature (~25 °C) by employing an Instron-type testing machine equipped with a strain gauge. The cross-head speed was established at 0.5 mm/min.

2.4. Corrosion resistance and ion release tests

Electrochemical corrosion test was conducted utilizing a standard three-electrode system immersed in a 0.9% NaCl solution at approximately 37 °C. The investigated sample was functioned as the working electrode with the saturated calomel electrode (SCE) and a Pt sheet as the reference electrode and counter electrode, correspondingly. Potentiodynamic polarization curves were measured by scanning the potential from –0.5 V (vs. SCE, unless differently indicated) to 2.8 V at a speed of 1 mV/s.

After immersing the sample in 30 mL of phosphate-buffered saline (PBS) at 37 °C for 24 hours, an inductively coupled plasma mass spectrometer (ICP-MS) was used to analyze the concentration of Cu^{2+} in the solution.

2.5. Cytocompatibility test

The toxicity of the sample was evaluated by MTT method using mouse embryonic osteoblast precursor cells (MC3T3-E1). The medium employed in this experiment consisted of α-minimum essential medium enriched with 10% fetal bovine serum. Samples with dimensions of 10 mm × 10 mm × 1.5 mm were subjected to mechanical polishing with sandpapers followed by thorough washing with deionized water, and finally sterilized at 121 °C for 30 min. Extraction was performed at 37 °C for 24 h according to ISO10993–12 standard with a surface area to liquid volume ratio of 1.25 cm^2/mL. The extracts were set up in 96-well plates separately. MC3T3-E1 cells were seeded into each well with the cell numbers of 2×10^3 cells/well for 24 h of incubation and 1×10^3 cells/well for 96 and 168 h of incubation. As a control group, MC3T3-E1 cells were seeded directly to the wells without extract. The 96-well plates were positioned in a humid incubator, maintained at a 37 °C and a 5% CO_2 atmosphere for 24, 96, and 168 h. After that, the samples were thoroughly washed three times with PBS. Then, 100 μL of culture solution that contained 10% MTT was infused into every well, followed by an additional 4 h of incubation at 37 °C and a 5% CO_2 atmosphere in the humid incubator. The liquid above the residue was removed, and 100 μL of dimethyl sulfoxide was added to each section, then gently shaken for 10 min. Optical density (OD) measurements were performed by using an enzyme marker at 570 nm.

2.6. Antibacterial properties

The antibacterial properties of the samples were evaluated by plate counting method using *E. coli* (ATCC25922) and *S. aureus* (ATCC29213) cells. The Ti–35Nb–(1, 2, 3, 4)Cu alloys were subjected to antibacterial tests with CP Ti as a control group. All samples were sterilized at 121 °C for 30 min in an autoclave, and then set into a 24-well plate. The bacterial solution was diluted to 10^6 CFU/mL by Luria-Bertani (LB) liquid medium, and 0.2 mL of the diluted bacterial solution was added to the surface of each sample. Sterile normal saline was added to the empty wells to prevent evaporation of water from the bacterial solution. The samples with suspension were incubated at 37 °C for 18 h, and then eluted by 1.8 mL sterile PBS to remove the bacteria solution on the surface. The eluent was then diluted 10^5 times by serial dilution. Afterward, 0.1 mL of each diluted solution was evenly applied on the LB solid medium in a Petri dish with diameter of 90 mm following by placing in a constant temperature incubator at 37°C for 18 hours. The number of colonies in the Petri dish was finally recorded. The antibacterial rate was calculated by the following formula (Eq. 1):

$$R = \frac{CFU_{\text{control}} - CFU_{\text{alloy}}}{CFU_{\text{control}}} \times 100\% \quad (1)$$

where CFU_{control} was the *CFU* of the control sample and CFU_{alloy} was *CFU* of the tested sample.

3. Results

3.1. Phase and microstructure

The XRD patterns of the solution-treated Ti–Nb–Cu alloys are shown in Fig. 1. The martensite transformation starting temperature (M_s) is approximately 160 °C in Ti–35 Nb [28]. Besides the peaks corresponding to β phase, the diffraction peaks of α" phase were found in the XRD pattern of Ti–35 Nb (Fig. 1a), because the β to α" martensite transformation occurred during quenching. The relative intensity of α" phase peaks became weak in the pattern of Ti–35Nb–1Cu (Fig. 1b), suggesting the martensite transformation also occurred. The Ti–35Nb–(2, 3, 4)Cu alloys only showed β phase peaks (Fig. 1c–e), indicating the martensite transformation hardly occurred during the cooling process.

The microstructures of solution-treated Ti–Nb–Cu alloys are shown in Fig. 2. Compared with the reported microstructure of Ti–35 Nb [27], the amount of needle-like α" phase in equiaxed β grains decreased in Ti–35Nb–1Cu (Fig. 2a). As the Cu content was further increased, only β

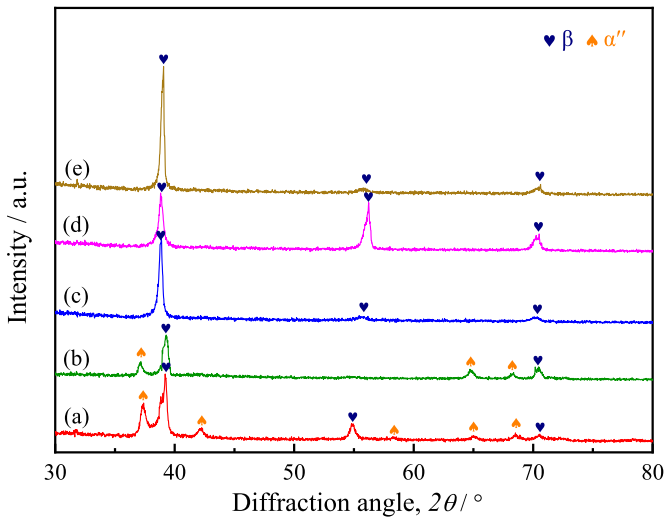

Fig. 1. XRD patterns of the solution-treated (a) Ti–35 Nb, (b) Ti–35Nb–1Cu, (c) Ti–35Nb–2Cu, (d) Ti–35Nb–3Cu, and (e) Ti–35Nb–4Cu.

grains were observed in Ti–35Nb–(2, 3, 4)Cu alloys (Fig. 2b–d). The microstructures well consistent with the XRD results, suggesting that Cu is a β stabilizer. It is concluded that the M_s of Ti–35Nb–1Cu is a little higher than room temperature, whereas the those of Ti–35Nb–(2, 3, 4) Cu alloys are all below room temperature.

3.2. Deformation behavior

The tensile stress-strain curves of the solution-treated Ti–35Nb–(0, 1, 2, 3, 4)Cu alloys are shown in Fig. 3. Ti–35 Nb and Ti–35Nb–1Cu exhibited a noticeable double yield phenomenon due to the widely recognized stress-induced martensitic transformation (SIMT) during the tensile process [29]. In their plastic deformation stages, the stress increased significantly with the increase of strain, indicating that Ti–35 Nb and Ti–35Nb–1Cu had a strong work hardening ability. With the increase of Cu content, the β phase stability was increased, the double yield phenomenon was hardly observed, and the work hardening ability gradually became weak.

The deformation bands in Ti–35 Nb alloy were determined as $\{332\}_\beta<113>_\beta$ twinning in the previous study [27]. For Ti–35Nb–1Cu alloy (Fig. 4a), similar deformation bands were also found by optical microscopy, and the amount of deformation bands decreased with the increase of Cu content (Fig. 4b–d), indicating that Cu suppressed the formation of twinning during tension. It was reported that twinning supplies dynamic reinforcement and increases the work-hardening rate [30]. Therefore, the reduction of work hardening ability was mainly due to the decrease of twinning. The change of deformation behavior also suggests that Cu works as a β stabilizer.

3.3. Mechanical properties

The mechanical properties of the solution-treated Ti–35Nb–(0, 1, 2, 3, 4)Cu alloys measured by tensile tests are presented in Fig. 5. Ti–35 Nb showed a 0.2% proof stress ($\sigma_{0.2}$) of approximately 400 MPa, an ultimate tensile strength (σ_b) of approximately 600 MPa, a Young's modulus (E) of approximately 72 GPa, and an elongation (ε_l) of approximately 30%. When the Cu content was increased to 1%, the $\sigma_{0.2}$, σ_b, and E decreased, and the ε_l increased. Ti–35 Nb consisted of β phase, ω phase, and α" phase, and exhibited the highest σ_b [27], because brittle ω phase brought precipitation strengthening. Both σ_b and $\sigma_{0.2}$ decreased in Ti–35Nb–1Cu

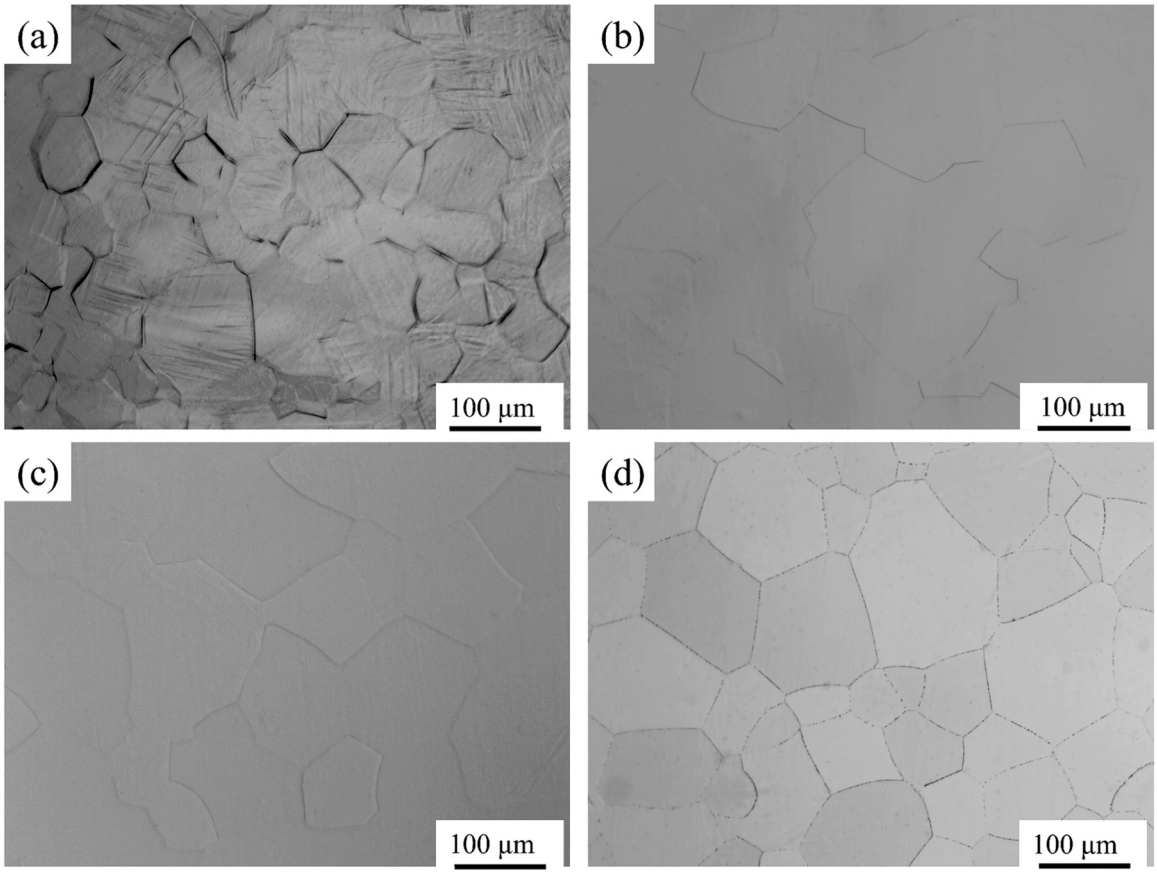

Fig. 2. Optical microstructures of the solution-treated (a) Ti–35Nb–1Cu, (b) Ti–35Nb–2Cu, (c) Ti–35Nb–3Cu, and (d) Ti–35Nb–4Cu.

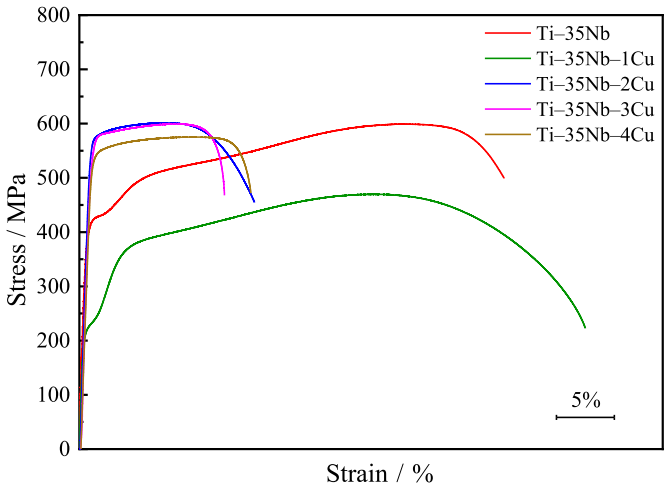

Fig. 3. Tensile stress-strain curves of the solution-treated Ti–35Nb–(0, 1, 2, 3, 4)Cu alloys.

owing to the decrease of ω phase. SIMT occurred in Ti–35 Nb and Ti–35Nb–1Cu with metastable β phase. The critical stress for inducing martensite was much lower than the yielding stress of β phase, so the $\sigma_{0.2}$ was much lower than σ_b. When the content of Cu was 2%, the β phase became stable, and the critical stress for inducing martensite was higher than the yielding stress of β phase, which meant with the increase of stress during tension, β phase yielded prior to SIMT [31]. Therefore, SIMT hardly occurred, and double yielding phenomenon disappeared. The $\sigma_{0.2}$ of Ti–35Nb–2Cu was related to the yielding of β phase. Meanwhile, the work hardening ability of Ti–35Nb–2Cu was weak; therefore, the $\sigma_{0.2}$ was just a little lower than σ_b. When the Cu content was continuously increased, noticeable increase of $\sigma_{0.2}$ or σ_b was hardly found, indicating that the solution strengthening effect of Cu was weak in the studied Ti–Nb–Cu alloys. Similar to Ti–35Nb–2Cu, the β phase was stable in Ti–35Nb–3Cu and Ti–35Nb–4Cu, so the σ_b was just a litter higher than $\sigma_{0.2}$.

Transformation induced plasticity (TRIP) and twinning induced plasticity (TWIP) were widely reported in the Ti alloys with metastable β phase [32,33]; therefore, Ti–35Nb–(0, 1)Cu alloys with SIMT and twinning showed the ε_l of more than 30%. As the Cu content was increased, the ε_l initially increased followed by a decline. The increase of

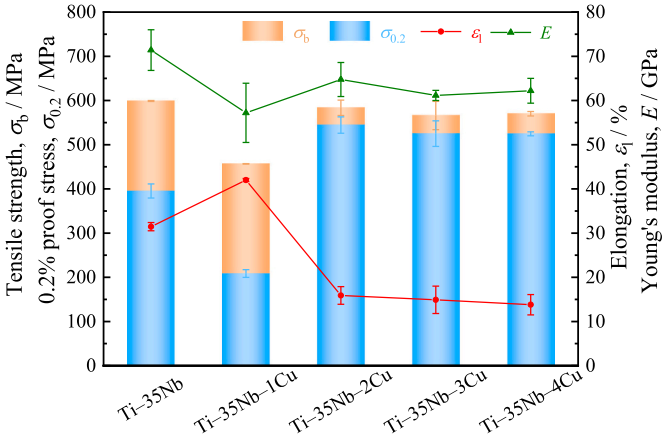

Fig. 5. Mechanical properties of the solution-treated Ti–35Nb–(0, 1, 2, 3, 4)Cu alloys measured by tensile tests.

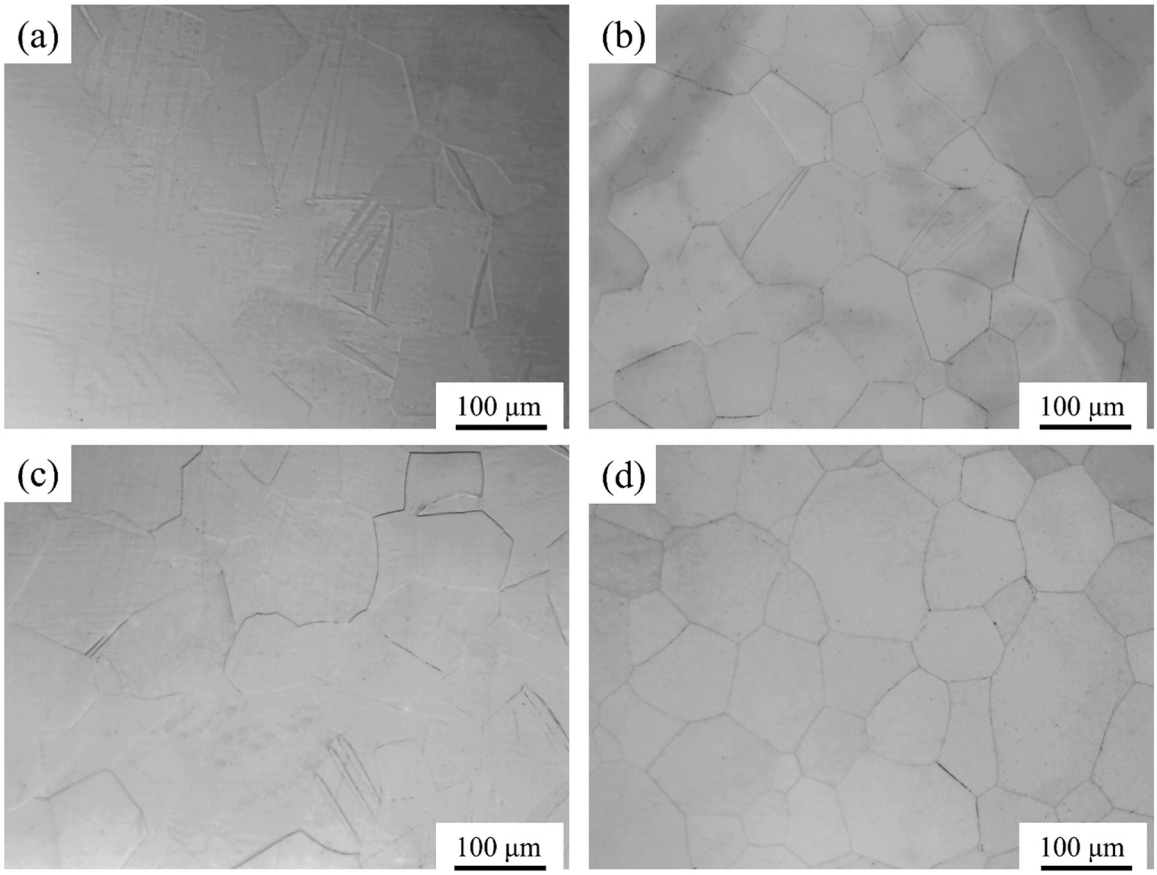

Fig. 4. Optical microstructures of (a) Ti–35Nb–1Cu, (b) Ti–35Nb–2Cu, (c) Ti–35Nb–3Cu, and (d) Ti–35Nb–4Cu after tensile tests.

ε_l in Ti–35Nb–1Cu was due to the disappearance of brittle ω phase. With the further increase of Cu content, the β phase stability was enhanced, and SIMT and twinning were suppressed. The disappearances of TRIP and TWIP were the main reasons for the decrease of ε_l in Ti–35Nb–2Cu. The weak solid solution strengthening of Cu rarely leaded to a great decrease in plasticity. The ε_l of Ti–35Nb–(2, 3, 4)Cu alloys were all approximately 15%, which was higher than those of other Cu added Ti–Nb alloys, such as Ti–6Nb–4Cu, Ti–18Nb–2Cu, and Ti–24Nb–1Cu [34].

The Young's modulus of the alloy is determined by the phase fraction and modulus of each phase. The phases in Ti alloys show different Young's moduli, and the order from high to low is ω > α > α′ > α" > β [35]. Ti–35 Nb exhibited a high Young's modulus of approximately 72 GPa owing to the exist of high-modulus ω phase [27]. It was well known that a lower Young's modulus would be obtained in the Ti alloy with the β phase in the transition between metastable state and stable state [36,37]. Cu could enhance the β phase stability, and inhibit the martensitic and ω phase transformations. Ti–35Nb–1Cu showed the lowest Young's modulus of ~57 GPa mainly owing to the inhibition of ω phase transformation, and Ti–35Nb–2Cu with a more stable β phase exhibits a higher Young's modulus of ~65 GPa. As the Cu content was further increased, the alloys consisted of a single β phase, and the Young's modulus was just slightly changed in Ti–35Nb–3Cu (~61.2 GPa) and Ti–35Nb–4Cu (~62.2 GPa).

3.4. Polarization curve

CP Ti and Ti–35Nb–(0, 1, 2, 3, 4)Cu alloys demonstrated similar passivation behaviors during polarization, as shown in Fig. 6. In the case of CP Ti, the current density initially dropped as the polarization potential was increased from –0.50 V. It reached the lowest point at –0.20 V, which was regarded as the corrosion potential (E_{corr}). When the polarization potential surpassed the corrosion potential, the current density increased and stabilized at approximately 0.47 V, indicating that a passivation behavior emerged, and a passive film developed on the surface. The almost steady current density was regarded as the primary passive current density (i_{pp}). When the polarization potential was raised to approximately 1.36 V, a spike of current density appeared, which was related to the appearance of pits caused by the breaking of the passive film. Subsequently, the current density gradually increased, indicating the passive film was partially dissolved or ruptured. At ~1.67 V, the current density was stable again, indicating that the sample entered a new passivation state. The Ti–35Nb–(0, 1, 2, 3, 4)Cu alloys showed similar corrosion behavior in the polarization curves. The results

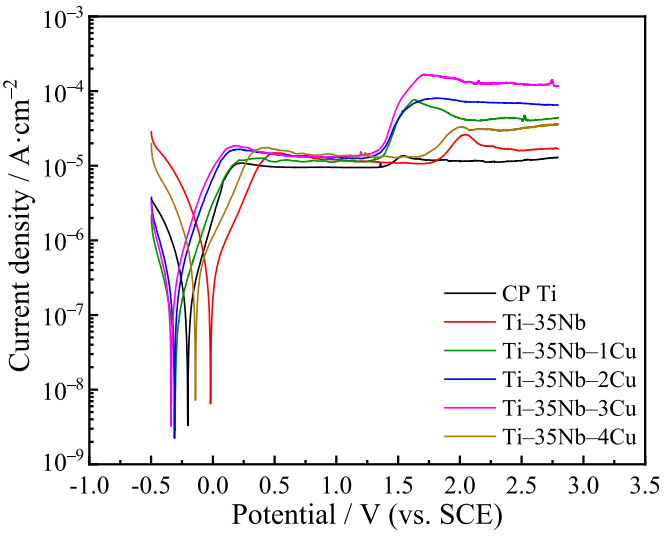

Fig. 6. Polarization curves of CP Ti and Ti–35Nb–(0, 1, 2, 3, 4)Cu alloys.

obtained from polarization curves are listed in Table 1. All the samples showed similar E_{corr}. The i_{pp} of Ti–35 Nb was 12.53 μA/cm^2, which was a little higher than that of CP Ti. With the increase of Cu, the i_{pp} marginally increased. Besides the higher i_{pp}, the current density curves of the Ti–Nb–Cu alloys were fluctuating in the primary passive state, and current density spikes appeared at lower potentials. This suggested that the corrosion behaviors were affected by the phase composition and Cu addition. Multi-phase Ti alloys usually have thinner passive films than those of single-phase Ti alloys, and the appearance of α" phase could make the alloy more active, resulting in an increase of i_{pp} [38,39]. The addition of Cu in Ti–Nb alloys decreased the stability of passive film, and thus increased i_{pp} [40,41]. Therefore, the Ti–35Nb–(0, 1)Cu alloys consisting of α"+β phases and the Ti–35Nb–(2, 3, 4)Cu alloys with more Cu showed a fluctuating i_{pp}, and their passive current densities were a little higher than that of CP Ti. Nevertheless, the passive current densities of the Ti–Nb–Cu alloys were similar to the other reported biomedical Ti alloys, such as Ti–15Mo (32.4 μA/cm^2), Ti–35Nb–7Zr–5Ta (~ 14 μA/cm^2) and Ti-13Nb-13Zr (~10 μA/cm^2) [42–44]. It was reported that the alloy would undergo self-passivation upon placement in the electrolyte, if the current density in the electrolyte fell below 100 μA/cm^2 [35]. Based on the potentiodynamic polarization results, the self-passive film formed on the surfaces of Ti–35Nb–(0, 1, 2, 3, 4)Cu alloys, and then prevented the continuous corrosion of the substrates.

3.5. Cu ion release

The Cu^{2+} release quantity of the sample in PBS slightly increased with the increase of Cu content in the alloy, as shown in Fig. 7. The Cu^{2+} concentration was ~0.017 μg/mL for Ti–35Nb–1Cu after immersing in the PBS for 24 hours, which was similar as Ti–2Cu [32]. When the Cu content was 4%, the Cu^{2+} concentration just increased to ~0.023 μg/mL. Although the Cu content in the alloy was multiply increased, the release quantity of Cu^{2+} did not proportionally increased. It could be attributed to the self-passivation behavior as mentioned above. The formation of passive film on the alloy surface enhanced the corrosion resistance and simultaneously impeded the release of Cu^{2+}.

3.6. Cytocompatibility

Fig. 8 shows the OD values of MC3T3-E1 cells corresponding to CP Ti, Ti–35Nb–(0, 1, 2, 3, 4)Cu alloys, and the control. After 24 h of incubation, all the samples and control showed similar cell viability. With the increase of incubation time, they all showed an increasing trend of cell viability. After 96 h of incubation, the OD values of alloys were all higher than that of the control. Especially, CP Ti, Ti–35Nb–2Cu and Ti–35Nb–3Cu showed significantly difference comparing with the control. After 168 h of incubation, the samples all showed considerably higher cell viability than that of the control, and the differences were all statistically significant. The OD value of CP Ti was the greatest, followed by Ti–35Nb–2Cu, indicating that the alloying elements in the Ti–Nb–Cu alloys might affect the cell viability. The OD values of Ti–35Nb–3Cu and Ti–35Nb–4Cu decreased in relation to Ti–35Nb–2Cu, possibly due to the slightly increasing release of Cu^{2+} from the alloys. Nevertheless, the OD values of the Ti–35Nb–(0, 1, 2, 3, 4)Cu alloys exceeded that of the

Table 1
Corrosion parameters of CP Ti and Ti–35Nb–(0, 1, 2, 3, 4)Cu alloys obtained from polarization curves.

Samples	E_{corr} (V, vs. SCE)	i_{pp} (μA/cm^2)
CP Ti	–0.20	9.54±0.11
Ti–35 Nb	–0.02	12.53±2.07
Ti–35Nb–1Cu	–0.31	12.06±0.69
Ti–35Nb–2Cu	–0.32	14.25±1.95
Ti–35Nb–3Cu	–0.34	15.41±2.59
Ti–35Nb–4Cu	–0.14	15.19±2.29

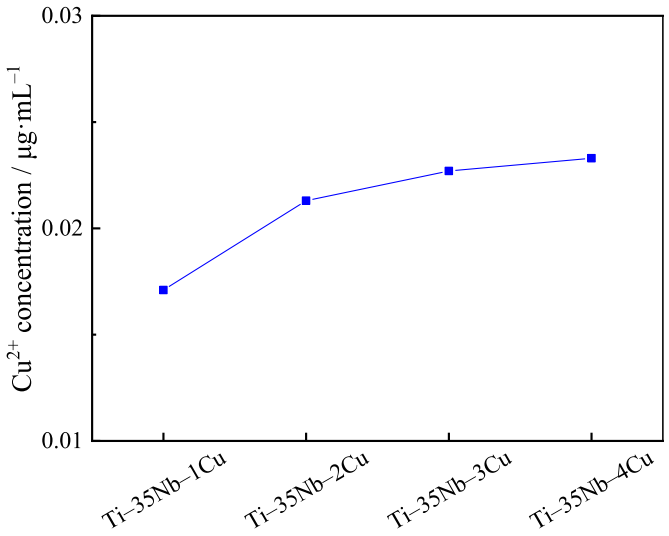

Fig. 7. Cu^{2+} concentrations in PBS after immersing for 24 h.

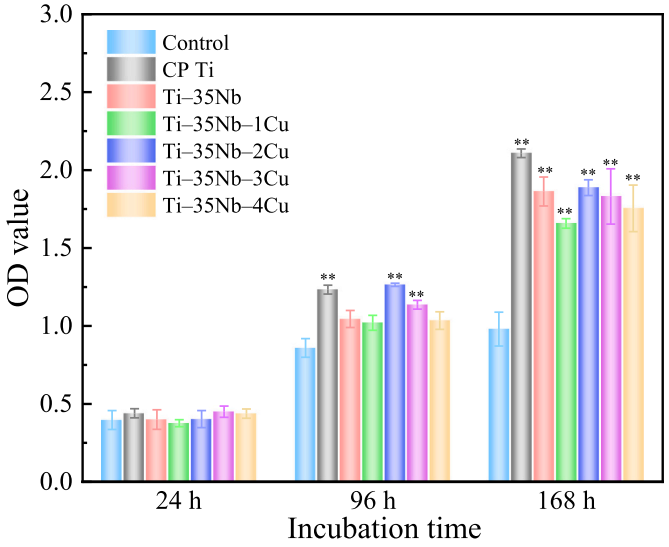

Fig. 8. OD values of MC3T3-E1 cells for CP Ti, Ti–35Nb–(0, 1, 2, 3, 4)Cu, and control after 24, 96, and 168 h of incubation (**denotes a significant difference at $P < 0.01$ compared to control).

control after 96 and 168 h of incubation, indicating that they possessed favorable cytocompatibility.

3.7. Antibacterial activity

Fig. 9 shows the colonies of *E. coli* and *S. aureus*. For CP Ti, numerous colonies were observed on the agar plates, which was consistent with the poor antibacterial properties of Ti and its alloys [45]. For the Ti–35Nb–(1, 2, 3, 4)Cu alloys, the number of colonies was significantly reduced, indicating that Cu enhanced the antibacterial properties and effectively suppressed the growth of *E. coli* and *S. aureus*. The antibacterial rates of Ti–35Nb–1Cu, Ti–35Nb–2Cu, and Ti–35Nb–3Cu and Ti–35Nb–4Cu alloys against *E. coli* were 62.8%, 68.9%, 70.9%, and 73.2%, respectively. Moreover, the antibacterial rates of Ti–35Nb–1Cu, Ti–35Nb–2Cu, Ti–35Nb–3Cu, and Ti–35Nb–4Cu alloys against *S. aureus* were 63.4%, 69.7%, 72.8% and 74.7%, respectively. With the increase of Cu content, the increase of antibacterial rate was attributed to the increase of Cu^{2+} release quantity, because Cu^{2+} was an effective ion to kill bacteria.

4. Discussion

The mechanical properties of Ti–Nb–Cu alloys were mainly determined by the phase composition and β phase stability, which were affected by the content of Cu. Ti_2Cu is a common intermetallic compound in Cu added Ti alloys [46]. It usually forms during ageing and significantly reduces the plasticity [47]. According to the Ti–Nb–Ti_2Cu pseudo-ternary phase diagram given by Sato, the Ti–35Nb–(1, 2, 3, 4)Cu should consist of a single β phase, and Ti_2Cu appeared with α phase in Ti–(5, 10)Nb–5Cu, but was hardly found in Ti–(20, 30)Nb–5Cu [48]. However, the β phase in Ti–35Nb–1Cu was metastable, and thus the α" martensite transformation occurred during quenching. The addition of Cu was no more than 4% in this study, which meant that the Cu content was lower than the critical content to form Ti_2Cu in Ti–35 Nb. The diffraction peak of Ti_2Cu was hardly found in the XRD patterns. Additionally, the Ti–35Nb–(2, 3, 4)Cu alloys all showed a stable β phase deformation behavior, and their elongations were much higher than those of Ti alloys with Ti_2Cu [22,47], which also suggested that the brittle Ti_2Cu phase hardly appeared.

It was reported that β-type Ti alloys with twinning generally exhibited low yield strength and large elongation [49]. Similar phenomena were also observed in the Ti–35Nb–(0, 1)Cu alloys. The double yield phenomenon disappeared in Ti–40 Nb (wt%) [50], Ti–35Nb–11Zr (wt%) [25], and Ti–35Nb–2Cu, suggesting that 2 wt% of Cu had a similar ability to stabilize β phase compared with 5 wt% of Nb and 11 wt % of Zr. As the Cu content was increased from 2% to 4%, the solid solution strengthening of Cu was rarely found according to the tensile test results, and the $\sigma_{0.2}$ and σ_b of Ti–35Nb–(2, 3, 4)Cu alloys were nearly the same and closed to other solution treated β-type Ti alloys, such as Ti–29Nb–13Ta–4.6Zr and Ti–35Nb–7Zr–5Ta. The addition of Cu did not cause a great increase in Young's modulus. The Young's moduli of Ti–35Nb–(3, 4)Cu alloys were both around 62 GPa, which was not inferior to other β-type Ti alloys. It suggests that desired mechanical properties can be obtained in the Cu added β-type Ti alloys, such as Ti–35Nb–4Cu in this study.

For metallic implants, corrosion is a common phenomenon after implantation, because the human environment is highly corrosive. Ti is reactive, but a compact passive film usually forms on the surface, which can prevent the severe corrosion. The corrosion properties of Ti and Ti alloys strongly depend on the stability of the passive film. The present study indicated the passive film prevented the transfer of ions from the substrate to the body fluid, and thus limited the release of Cu^{2+}. The antibacterial properties of Cu added Ti alloys are mainly attributed to the release of Cu^{2+}, and the appearance of Ti_2Cu accelerates the release and improves the antibacterial rate [22]. Although Ti_2Cu was hardly found in the solution-treated Ti–35Nb–(1, 2, 4)Cu alloys, the alloys also showed considerable antibacterial properties. The antibacterial rates of the Ti–Nb–Cu alloys against *E. coli* were near to those of Ti–(2, 3, 4)Cu alloys containing Ti_2Cu [51].

Overall, Cu has a melting point near to Ti, and shows a higher ability to stabilize β phase, which can reduce the amount of other β stabilizers with higher melting points. As the Cu content was increased to 4%, Ti–Cu intermetallic compounds were hardly found in the studied Ti–Nb–Cu alloys, and all the alloys showed good plasticity. The self-passive film on the surface ensured a good corrosion resistance of the alloy, and resulted in a slow releasing of Cu^{2+}, which made a balance between antibacterial activity and biocompatibility. The addition of low-price Cu is benefit to reduce the cost of β-type Ti alloys. Based on the prices of the elements published by Nilaco Japan on 17 January 2024 [52], the raw material costs of Ti–35Nb–(1, 2, 3, 4)Cu alloys are approximately 3246–3490 USD/kg, which are low than those of Ti–29Nb–13Ta–4.6Zr (3657 USD/kg) and Ti–35Nb–7Zr–5Ta (3573 USD/kg). Ti–35Nb–4Cu with a Young's modulus of approximately 62 GPa, a tensile strength of approximately 570 MPa, and an elongation of approximately 15% is a prospective antibacterial material for hard tissue replacements.

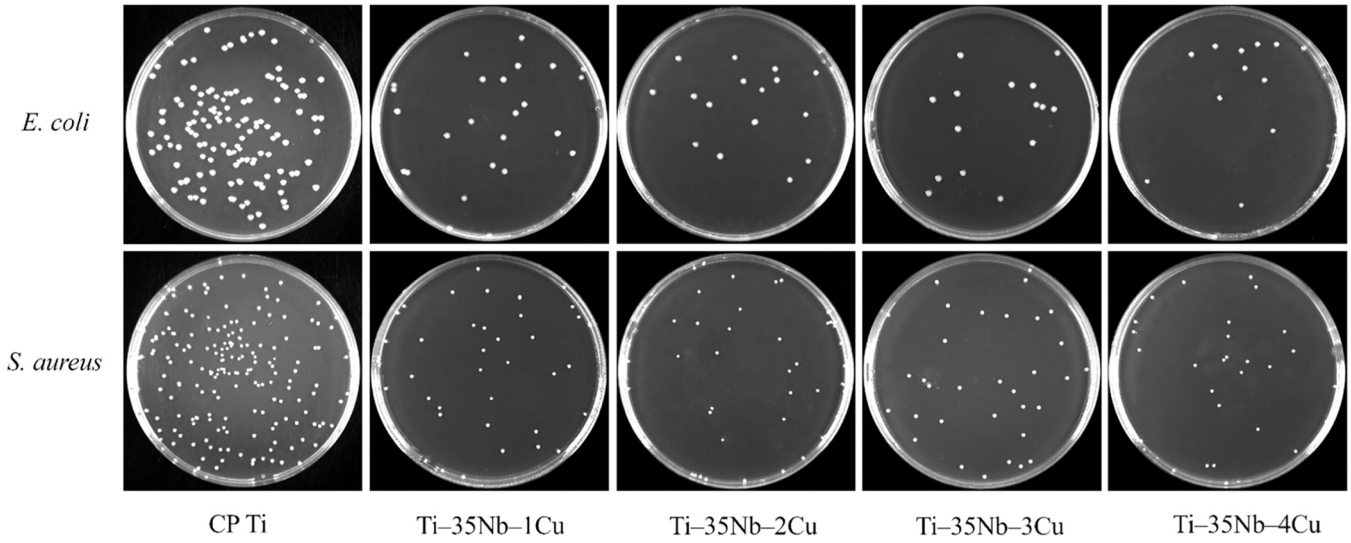

Fig. 9. Morphologies of *E. coli* and *S. aureus* colonies.

5. Conclusions

The following conclusions can be obtained based on the above results and discussions:

(1) Cu inhibited the ω and α" transformations in Ti–35 Nb during quenching, and suppressed SIMT and twinning during tension. SIMT was observed in the Ti–35Nb–(0, 1)Cu alloys, but the Ti–35Nb–(2, 3, 4)Cu alloys showed stable-β-phase deformation behaviors and similar mechanical properties.

(2) The Ti–35Nb–(1, 2, 3, 4)Cu alloys showed similar corrosion behavior and cytocompatibility compared with CP Ti. Passive films formed on the surfaces and limited the release of Cu^{2+} from the alloys. The Cu added Ti–Nb alloys inhibited the growth of *E. coli* and *S. aureus*, and exhibited good biocompatibility.

(3) The solution-treated Ti–35Nb–4Cu showed desirable comprehensive mechanical properties and antibacterial properties; therefore, it is suitable for biomedical applications.

CRediT authorship contribution statement

Qiang Li: Writing – review & editing, Writing – original draft, Investigation, Funding acquisition. **Qi Huang:** Resources, Investigation. **Qizhen Peng:** Writing – review & editing, Writing – original draft, Investigation. **Takuya Ishimoto:** Investigation. **Mitsuo Niinomi:** Investigation, Funding acquisition. **Takayoshi Nakano:** Investigation.

Declaration of Competing Interest

The authors declare that they have no known competing financial interests or personal relationships that could have appeared to influence the work reported in this paper.

Data availability

Data will be made available on request.

Acknowledgements

This work was partially supported by Shanghai Engineering Research Center of High-Performance Medical Device Materials (No. 20DZ2255500), and the Grant-in Aid for Scientific Research (C) (No. 20K05139) from Japan Society for the Promotion of Science, Tokyo, Japan.

References

[1] S. Ehtemam-Haghighi, Y. Liu, G. Cao, L.-C. Zhang, Phase transition, microstructural evolution and mechanical properties of Ti-Nb-Fe alloys induced by Fe addition, Mater. Des. 97 (2016) 279–286, https://doi.org/10.1016/j.matdes.2016.02.094.
[2] Q.-K. Meng, Y.-F. Huo, W. Ma, Y.-W. Sui, J.-Y. Zhang, S. Guo, X.-Q. Zhao, Design and fabrication of a low modulus β-type Ti–Nb–Zr alloy by controlling martensitic transformation, Rare Met. 37 (2018) 789–794, https://doi.org/10.1007/s12598-018-1055-5.
[3] D.-K. Kang, S.-K. Moon, K.-T. Oh, G.-S. Choi, K.-N. Kim, Properties of experimental titanium-silver-copper alloys for dental applications, J. Biomed. Mater. Res B Appl. Biomater. 90B (2009) 446–451, https://doi.org/10.1002/jbm.b.31305.
[4] C.M. Suryawanshi, B. Gaur, A.K. Singh, D. Soman, S. Sagar, R. Bhallamudi, S. Mishra, Microstructure and mechanical characterization of direct metal laser sintered Ti-6Al-4V alloy for orthopedic implant applications, Mater. Today Commun. 35 (2023) 105770, https://doi.org/10.1016/j.mtcomm.2023.105770.
[5] L. Zhang, L. Chen, A review on biomedical titanium alloys: recent progress and prospect, Adv. Eng. Mater. 21 (2019), https://doi.org/10.1002/adem.201801215.
[6] M. Niinomi, M. Nakai, Titanium-based biomaterials for preventing stress shielding between implant devices and bone, Int J. Biomater. 2011 (2011) 1–10, https://doi.org/10.1155/2011/836587.
[7] S.E. Haghighi, H.B. Lu, G.Y. Jian, G.H. Cao, D. Habibi, L.C. Zhang, Effect of α″ martensite on the microstructure and mechanical properties of beta-type Ti–Fe–Ta alloys, Mater. Des. 76 (2015) 47–54, https://doi.org/10.1016/j.matdes.2015.03.028.
[8] J. Wang, W. Xiao, L. Ren, Y. Fu, C. Ma, The roles of oxygen content on microstructural transformation, mechanical properties and corrosion resistance of Ti-Nb-based biomedical alloys with different β stabilities, Mater. Charact. 176 (2021) 111122, https://doi.org/10.1016/j.matchar.2021.111122.
[9] M. Niinomi, M. Nakai, J. Hieda, Development of new metallic alloys for biomedical applications, Acta Biomater. 8 (2012) 3888–3903, https://doi.org/10.1016/j.actbio.2012.06.037.
[10] M. Hendrickson, S.A. Mantri, Y. Ren, T. Alam, V. Soni, B. Gwalani, M. Styles, D. Choudhuri, R. Banerjee, The evolution of microstructure and microhardness in a biomedical Ti–35Nb–7Zr–5Ta alloy, J. Mater. Sci. 52 (2017) 3062–3073, https://doi.org/10.1007/s10853-016-0591-3.
[11] K.C. Nune, R.D.K. Misra, S.J. Li, Y.L. Hao, R. Yang, Osteoblast cellular activity on low elastic modulus Ti–24Nb–4Zr–8Sn alloy, Dent. Mater. 33 (2017) 152–165, https://doi.org/10.1016/j.dental.2016.11.005.
[12] D. Xu, T. Wang, S. Wang, Y. Jiang, Y. Wang, Y. Chen, Z. Bi, S. Geng, Antibacterial effect of the controlled nanoscale precipitates obtained by different heat treatment schemes with a Ti-based nanomaterial, Ti–7.5Mo–5Cu alloy, ACS Appl. Bio Mater. 3 (2020) 6145–6154, https://doi.org/10.1021/acsabm.0c00716.
[13] O. Mazigi, M.B. Kannan, J. Xu, H.-C. Choe, Q. Ye, Biocompatibility and degradation of a low elastic modulus Ti-35Nb-3Zr Alloy: nanosurface engineering for enhanced degradation resistance, ACS Biomater. Sci. Eng. 3 (2017) 509–517, https://doi.org/10.1021/acsbiomaterials.6b00563.
[14] A. Burla, M. Khandelwal, M. Vaidya, Antibacterial properties of Cu containing complex concentrated alloys, Mater. Today Commun. 33 (2022) 104915, https://doi.org/10.1016/j.mtcomm.2022.104915.
[15] S.J.A. Zaidi, S. Zoha, M. Ahmad, M. Shahid, T.J. Park, M.A. Basit, Physicochemically tailored Ag2S QDs deposition on ZnO for improved photocatalytic and antibacterial performance, Mater. Today Commun. 37 (2023) 107016, https://doi.org/10.1016/j.mtcomm.2023.107016.
[16] Y. Feng, G. Wang, Y. Chang, Y. Cheng, B. Sun, L. Wang, C. Chen, H. Zhang, Electron compensation effect suppressed silver Ion release and contributed safety of Au@Ag

core–shell nanoparticles, Nano Lett. 19 (7) (2019) 4478–4489, https://doi.org/10.1021/acs.nanolett.9b01293.
[17] L. Ren, K. Yang, L. Guo, H.-w Chai, Preliminary study of anti-infective function of a copper-bearing stainless steel, Mater. Sci. Eng. C 32 (5) (2012) 1204–1209, https://doi.org/10.1016/j.msec.2012.03.009.
[18] S. Wang, C. Yang, L. Ren, M. Shen, K. Yang, Study on antibacterial performance of Cu-bearing cobalt-based alloy, Mater. Lett. 129 (2014) 88–90, https://doi.org/10.1016/j.matlet.2014.05.020.
[19] Y. Li, H. Wang, K. Koenigsmann, H. Liu, S. Zhang, L. Ren, K. Yang, Ultrafine-grained Ti6Al7Nb-xCu alloy with ultrahigh strength and exceptional biomedical properties, J. Mater. Sci. Technol. 164 (2023) 68–78, https://doi.org/10.1016/j.jmst.2023.04.035.
[20] Z. Ma, M. Yao, R. Liu, K. Yang, L. Ren, Y. Zhang, Z. Liao, W. Liu, M. Qi, Study on antibacterial activity and cytocompatibility of Ti–6Al–4V–5Cu alloy, Mater. Technol. 30 (sup6) (2015) B80–B85, https://doi.org/10.1179/1753555714Y.0000000237.
[21] S.K. Kolawole, W. Hai, S. Zhang, Z. Sun, M.A. Siddiqui, I. Ullah, W. Song, F. Witte, K. Yang, Preliminary study of microstructure, mechanical properties and corrosion resistance of antibacterial Ti-15Zr-xCu alloy for dental application, J. Mater. Sci. Technol. 50 (2020) 31–43, https://doi.org/10.1016/j.jmst.2020.03.003.
[22] H.-L. Yang, M.-Z. Zhu, J.-Y. Wang, C.-X. Ma, X.-W. Zhou, H.-X. Xing, E.-L. Zhang, S.-X. Ji, Optimization of mechanical and antibacterial properties of Ti-3wt%Cu alloy through cold rolling and annealing, Rare Met. 41 (2022) 610–620, https://doi.org/10.1007/s12598-021-01841-x.
[23] D.P. de Andrade, L.M.R. de Vasconcellos, I.C.S. Carvalho, L.F. de, B.P. Forte, E.L. de Souza Santos, R.F. do Prado, D.R. dos Santos, C.A.A. Cairo, Y.R. Carvalho, Titanium–35niobium alloy as a potential material for biomedical implants: In vitro study, Mater. Sci. Eng. C 56 (2015) 538–544, https://doi.org/10.1016/j.msec.2015.07.026.
[24] A.R. Luz, G.B. de Souza, C.M. Lepienski, C.J.M. Siqueira, N.K. Kuromoto, Tribological properties of nanotubes grown on Ti-35Nb alloy by anodization, Thin Solid Films 660 (2018) 529–537, https://doi.org/10.1016/j.tsf.2018.06.050.
[25] J.I. Kim, H.Y. Kim, T. Inamura, H. Hosoda, S. Miyazaki, Shape memory characteristics of Ti–22Nb–(2–8)Zr(at%) biomedical alloys, Mater. Sci. Eng. A 403 (2005) 334–339, https://doi.org/10.1016/j.msea.2005.05.050.
[26] H.Y. Kim, S. Hashimoto, J.I. Kim, T. Inamura, H. Hosoda, S. Miyazaki, Effect of Ta addition on shape memory behavior of Ti–22Nb alloy, Mater. Sci. Eng. A 417 (2006) 120–128, https://doi.org/10.1016/j.msea.2005.10.065.
[27] Q. Li, G. Ma, J. Li, M. Niinomi, M. Nakai, Y. Koizumi, D.-X. Wei, T. Kakeshita, T. Nakano, A. Chiba, X. Liu, K. Zhou, D. Pan, Development of low-Young's modulus Ti–Nb-based alloys with Cr addition, J. Mater. Sci. 54 (2019) 8675–8683, https://doi.org/10.1007/s10853-019-03457-0.
[28] H.Y. Kim, S. Hashimoto, J.I. Kim, H. Hosoda, S. Miyazaki, Mechanical properties and shape memory behavior of Ti-Nb Alloys, Mater. Trans. 45 (7) (2004) 2443–2448, https://doi.org/10.2320/matertrans.45.2443.
[29] H.-S. Kim, S.-H. Lim, I.-D. Yeo, W.-Y. Kim, Stress-induced martensitic transformation of metastable β-titanium alloy, Mater. Sci. Eng. A 449–451 (2007) 322–325, https://doi.org/10.1016/j.msea.2006.02.329.
[30] M. Weiss, K. Mester, A. Taylor, N. Stanford, A critical assessment of deformation twinning and epsilon martensite formation in austenitic alloys during complex forming operations, Mater. Charact. 145 (2018) 423–434, https://doi.org/10.1016/j.matchar.2018.09.003.
[31] K.M. Kim, H.Y. Kim, S. Miyazaki, Effect of Zr content on phase stability, deformation behavior, and Young's modulus in Ti–Nb–Zr alloys, Materials 13 (2) (2020) 476, https://doi.org/10.3390/ma13020476.
[32] J. Liu, F. Li, C. Liu, H. Wang, B. Ren, K. Yang, E. Zhang, Effect of Cu content on the antibacterial activity of titanium–copper sintered alloys, Mater. Sci. Eng. C 35 (2014) 392–400, https://doi.org/10.1016/j.msec.2013.11.028.
[33] H. Dong, Z.C. Li, M.C. Somani, R.D.K. Misra, The significance of phase reversion-induced nanograined/ultrafine-grained (NG/UFG) structure on the strain hardening behavior and deformation mechanism in copper-bearing antimicrobial austenitic stainless steel, J. Mech. Behav. Biomed. Mater. 119 (2021) 104489, https://doi.org/10.1016/j.jmbbm.2021.104489.
[34] M. Takahashi, M. Kikuchi, Y. Takada, Mechanical properties and microstructures of dental cast Ti-6Nb-4Cu, Ti-18Nb-2Cu, and Ti-24Nb-1Cu alloys, Dent. Mater. J. 35 (2016) 564–570, https://doi.org/10.4012/dmj.2015-354.
[35] C.M. Lee, C.P. Ju, J.H. Chern Lin, Structure-property relationship of cast Ti-Nb alloys, J. Oral. Rehabil. 29 (2002) 314–322, https://doi.org/10.1046/j.1365-2842.2002.00825.x.
[36] Y.L. Hao, S.J. Li, S.Y. Sun, R. Yang, Effect of Zr and Sn on Young's modulus and superelasticity of Ti–Nb-based alloys, Mater. Sci. Eng. A 441 (2006) 112–118, https://doi.org/10.1016/j.msea.2006.09.051.
[37] M. Abdel-Hady, K. Hinoshita, M. Morinaga, General approach to phase stability and elastic properties of β-type Ti-alloys using electronic parameters, Scr. Mater. 55 (2006) 477–480, https://doi.org/10.1016/j.scriptamat.2006.04.022.
[38] A. Cremasco, W.R. Osório, C.M.A. Freire, A. Garcia, R. Caram, Electrochemical corrosion behavior of a Ti–35Nb alloy for medical prostheses, Electro Acta 53 (14) (2008) 4867–4874, https://doi.org/10.1016/j.electacta.2008.02.011.
[39] X.H. Min, S. Emura, T. Nishimura, L. Zhang, S. Tamilselvi, K. Tsuchiya, K. Tsuzaki, Effects of α phase precipitation on crevice corrosion and tensile strength in Ti–15Mo alloy, Mater. Sci. Eng. A 527 (6) (2010) 1480–1488, https://doi.org/10.1016/j.msea.2009.10.033.
[40] I. Çaha, A.C. Alves, C. Chirico, A. Maria Pinto, S. Tsipas, E. Gordo, O. Bondarchuk, F. Leonard Deepak, F. Toptan, Atomic–scale investigations of passive film formation on Ti-Nb alloys, Appl. Surf. Sci. 615 (2023) 156282, https://doi.org/10.1016/j.apsusc.2022.156282.
[41] I. Mutlu, E. Oktay, Localised corrosion behaviour of biomedical implant materials using electrochemical potentiokinetic reactivation and critical pitting potential methods, Corros. Eng. Sci. Technol. 50 (1) (2015) 72–79, https://doi.org/10.1179/1743278214Y.0000000192.
[42] S. Kumar, T.S.N. Sankara Narayanan, Electrochemical characterization of β-Ti alloy in Ringer's solution for implant application, J. Alloy. Compd. 479 (1) (2009) 699–703, https://doi.org/10.1016/j.jallcom.2009.01.036.
[43] J.M. Cordeiro, B.E. Nagay, A.L.R. Ribeiro, N.C. da Cruz, E.C. Rangel, L.M.G. Fais, L. G. Vaz, V.A.R. Barão, Functionalization of an experimental Ti-Nb-Zr-Ta alloy with a biomimetic coating produced by plasma electrolytic oxidation, J. Alloy. Compd. 770 (2019) 1038–1048, https://doi.org/10.1016/j.jallcom.2018.08.154.
[44] S.L. Assis, S. Wolynec, I. Costa, The electrochemical behaviour of Ti-13Nb-13Zr alloy in various solutions, Mater. Corros. 59 (9) (2008) 739–743, https://doi.org/10.1002/maco.200804148.
[45] E. Zhang, F. Li, H. Wang, J. Liu, C. Wang, M. Li, K. Yang, A new antibacterial titanium–copper sintered alloy: preparation and antibacterial property, Mater. Sci. Eng. C 33 (2013) 4280–4287, https://doi.org/10.1016/j.msec.2013.06.016.
[46] K. Dyal Ukabhai, U.A. Curle, N.D.E. Masia, M. Smit, I.A. Mwamba, S. Norgren, C. Öhman-Mägi, N.G. Hashe, L.A. Cornish, Formation of Ti2Cu in Ti-Cu Alloys, J. Phase Equilib. Diffus 43 (3) (2022) 332–344, https://doi.org/10.1007/s11669-022-00964-7.
[47] Z. Wang, B. Fu, Y. Wang, T. Dong, J. Li, G. Li, X. Zhao, J. Liu, G. Zhang, Effect of Cu content on the precipitation behaviors, mechanical and corrosion properties of as-cast Ti-Cu alloys, Materials 15 (2022) 1696, https://doi.org/10.3390/ma15051696.
[48] K. Sato, M. Takahashi, Y. Takada, Construction of Ti-Nb-Ti_2Cu pseudo-ternary phase diagram, Dent. Mater. J. 39 (3) (2020) 422–428, https://doi.org/10.4012/dmj.2018-394.
[49] C.D. Rabadia, S.F. Jawed, J. Wang, M. Siddhpura, A. Siddhpura, Revised semiempirical approach to predict the occurrence of twinning in titanium alloys, ACS Omega 6 (2021) 34056–34064, https://doi.org/10.1021/acsomega.1c05474.
[50] A. Helth, S. Pilz, T. Kirsten, L. Giebeler, J. Freudenberger, M. Calin, J. Eckert, A. Gebert, Effect of thermomechanical processing on the mechanical biofunctionality of a low modulus Ti-40Nb alloy, J. Mech. Behav. Biomed. Mater. 65 (2017) 137–150, https://doi.org/10.1016/j.jmbbm.2016.08.017.
[51] E. Zhang, J. Ren, S. Li, L. Yang, G. Qin, Optimization of mechanical properties, biocorrosion properties and antibacterial properties of as-cast Ti–Cu alloys, Biomed. Mater. 11 (2016) 065001, https://doi.org/10.1088/1748-6041/11/6/065001.
[52] Nilaco. Pure Metals. Available online: ⟨https://shop.nilaco.jp/en/order/?large_category=1⟩ (accessed on 17 January 2024).